

# Relativistic Tearing and Drift-kink Instabilities in Two-fluid Simulations

Maxim V. Barkov<sup>1\*</sup> and Serguei S. Komissarov<sup>2†</sup>

<sup>1</sup> *Astrophysical Big Bang Laboratory, RIKEN, 351-0198 Saitama, Japan*

<sup>2</sup> *Department of Applied Mathematics, The University of Leeds, Leeds, LS2 9JT*

Received/Accepted

## ABSTRACT

The stability of current sheets in collisionless relativistic pair plasma was studied via two-dimensional two-fluid relativistic magnetohydrodynamic simulations with vanishing internal friction between fluids. In particular, we investigated the linear growth of the tearing and drift-kink modes in the current sheets both with and without the guide field and obtained the growth rates which are very similar to what has been found in the corresponding PIC simulations. This suggests that the two-fluid simulations can be useful in studying the large-scale dynamics of astrophysical relativistic plasmas in problems involving magnetic reconnection.

**Key words:** magnetic fields – plasmas – relativistic processes – MHD – waves – methods: numerical

## 1 INTRODUCTION

It is now well recognised that magnetic field is a “major player” in the dynamics of astrophysical plasma – the Lorentz force shapes a wide variety of flows in the Universe. The dissipative effects are also important, leading to magnetic reconnection and explosive release of stored magnetic energy. This could be of particular relevance in the astrophysics of neutron stars and black holes, which are expected to produce relativistic magnetically-dominated plasma. Magnetic reconnection accompanied by dissipation of magnetic energy may be the main processes leading to the observed non-thermal emission from winds and jets produced by these compact relativistic objects (e.g. Romanova & Lovelace 1992; Drenkhahn & Spruit 2002; Lyutikov & Blandford 2003; Zhang & Yan 2011; McKinney & Uzdensky 2012; Komissarov 2013; Porth et al. 2013, 2014).

The magnetic dissipation associated with the magnetic reconnection is not captured in the framework of ideal relativistic MHD, which is currently the most common tool of modelling astrophysical phenomena. The approximation of resistive MHD does introduce Ohmic dissipation of magnetic field but the astrophysical plasmas are often collisionless, whereas the resistivity has strong physical justification only for collisional plasmas.

Kinetic models of plasma are better suited in fundamental physics and more suitable for collisionless plasma but they are also much more complex and computationally expensive. PIC-simulations, based on dynamics of individual particles (or rather “super-particles”), are also quite expensive. Studies based on these methods shows that fast magnetic reconnection involves development of current sheets whose thickness is comparable to the electron skin depth, the kinetic scale absent in single fluid MHD (Zenitani & Hoshino 2001, 2007; Bessho & Bhattacharjee 2012; Cerutti et al. 2014; Sironi & Spitkovsky 2014; Liu et al. 2015).

Half-way between these frameworks and the single fluid MHD are the multi-fluid models, where plasma is considered as a collection of several inter-penetrating charged and neutral fluids, coupled via macroscopic electromagnetic field. Like a single fluid MHD, this approach is well suited for studying the large-scale dynamics of plasma flows. Moreover, it also captures some elements of plasma microphysics in the form of collective interaction between its positively and negatively charged components, which leads to the emergence of the plasma frequency and electron skin depth. Its generalised Ohm’s law has several terms which introduce non-ideal properties even in the absence of explicit internal friction between fluids. For this reason, the multi-fluid approximation is considered as a potential alternative to more expensive kinetic and PIC approaches when it comes to problems of macroscopic plasma dynamics where the magnetic reconnection plays an important dynamic role via restructuring of magnetic field and magnetic dissipation. For relativistic plasma, created in magnetospheres

\* E-mail: maxim.barkov@riken.jp (MVB)

† E-mail: S.S.Komissarov@leeds.ac.uk (SSK)

of neutron stars and black holes via various pair production processes, a simple two-fluid approximation involving electron and positron fluids may be sufficient. Obviously, the lack of spectral information means that the fluid framework has rather limited potential for addressing such important issues as radiation and non-thermal particle acceleration.

So far, there has been only a rather limited effort to explore the potential of the two-fluid approximation in numerical modelling of relativistic plasma. Zenitani et al. (2009a,b) used this approach for studying the relativistic magnetic reconnection, Amano & Kirk (2013) to study the termination shocks of pulsar winds, and Kojima & Oogi (2009) tried to construct two-fluid models of steady-state pulsar magnetospheres. In the same way as this is done in resistive MHD simulations, Zenitani et al. (2009b,a) used anomalous resistivity to trigger fast magnetic reconnection of Petschek-type. However, they noticed that the inertial terms of the generalised Ohm's law also make a significant contribution to the reconnection electric field, even exceeding that of the friction term, which represents the resistivity. Based on this observation, they suggested that the inertial terms alone may be sufficient to sustain magnetic reconnection. The robustness of this conclusion is not clear as they have also found that the simulations outcome strongly depends on the model of resistivity. Moreover, they used the Lax-Wendroff numerical scheme which also introduces numerical resistivity, whose contribution to the reconnecting electric field exceeds the other terms Zenitani et al. (2009b,a). However, if the two-fluid model can reproduce the reconnection rate sufficiently accurately then this approach becomes very useful for studying large-scale phenomena where magnetic restructuring and dissipation are important dynamical factors.

Until recently, the fast magnetic reconnection was viewed in the context of the Petschek model with its compact diffusion zone, as opposed to the slow Sweet-Parker type reconnection of long and thin current sheets. However, long current sheets are unstable to tearing mode instability (TI), which splits it into much shorter current sheets separated by plasmoids. 2D simulations discovered that at the non-linear stage the current sheet becomes highly dynamic, with mergers of original plasmoids and creation of new ones. This leads to a much higher overall reconnection rate (e.g. Biskamp 1986; Shibata & Tanuma 2001; Loureiro et al. 2007; Bhattacharjee et al. 2009; Uzdensky et al. 2010). In addition to TI, currents sheets are also subject to the so-called drift-kink instability (DKI) which grows faster (Zenitani & Hoshino 2007; Cerutti et al. 2014). This discovery suggested that DKI may hinder the development of TI. However, recent 3D PIC simulations, where both types of modes are allowed, show that TI is not suppressed and becomes dominant at the non-linear phase. The reconnection rates in 3D and 2D simulations are found to be similar (Sironi & Spitkovsky 2014; Liu et al. 2015).

Given the importance of TI and DK instabilities in the fast magnetic reconnection, the potential of the two-fluid model depends on how well it can describe their development. In this paper, we focus on the linear development of these instabilities numerically. To this aim, we used our recently developed two-fluid code for pair plasma (JANUS, Barkov et al. 2014). This code is based on a Godunov-type numerical scheme which is much less dissipative compared to the Lax-Wendroff one. It is third-order accurate in smooth regions, which makes it powerful tool for studying the instabilities. By setting the internal friction between the fluids (the resistivity) to zero we focus on the role of the inertial terms in the generalised Ohm's law. The results are compared with the growth rates obtained via PIC simulations by other groups. In the follow-up paper, we will discuss the nonlinear phases of magnetic reconnection in the plasmoid-dominated regime.

## 2 TWO-FLUID MODEL OF PAIR PLASMA

Following Zenitani et al. (2009a) we adopt the 3+1 (- +++) Special Relativistic equations originated from the covariant formulation by Gurovich & Solov'ev (1986). The corresponding dimensionless equations are (for details see Barkov et al. 2014)

- the continuity equations

$$\partial_t(n_{\pm}\gamma_{\pm}) + \nabla_i(n_{\pm}u_{\pm}^i) = 0; \quad (1)$$

- the total energy equation

$$\partial_t \left( \sum_{\pm} (w_{\pm}\gamma_{\pm}^2 - p_{\pm}) + \frac{\mathcal{K}_q}{2\mathcal{K}_m} (B^2 + E^2) \right) + \nabla_i \left( \sum_{\pm} w_{\pm}\gamma_{\pm}u_{\pm}^i + \frac{\mathcal{K}_q}{\mathcal{K}_m} e^{ijk} E_j B_k \right) = 0; \quad (2)$$

- the total momentum equation

$$\partial_t \left( \sum_{\pm} w_{\pm}\gamma_{\pm}u_{\pm}^s + \frac{\mathcal{K}_q}{\mathcal{K}_m} e^{sjk} E_j B_k \right) + \nabla_i \left( \sum_{\pm} (w_{\pm}u_{\pm}^i u_{\pm}^s + p_{\pm}g^{is}) + \frac{\mathcal{K}_q}{\mathcal{K}_m} \left( -E^i E^s - B^i B^s + \frac{1}{2} (B^2 + E^2) g^{is} \right) \right) = 0; \quad (3)$$

- the Maxwell equations

$$\nabla_i B^i = 0, \quad (4)$$

$$\partial_t B^s + e^{sik} \partial_i E_k = 0, \quad (5)$$

$$\nabla_i E^i = \frac{1}{\mathcal{K}_q} (n_+ \gamma_+ - n_- \gamma_-), \quad (6)$$

$$\partial_t E^s - e^{sik} \partial_i B_k = -\frac{1}{\mathcal{K}_q} (n_+ u_+^s - n_- u_-^s). \quad (7)$$

- and the generalised Ohm's law

$$\partial_t \left( \sum_{\pm} \pm w_{\pm} \gamma_{\pm} u_{\pm}^s \right) + \nabla_i \left( \sum_{\pm} \pm (w_{\pm} u_{\pm}^i u_{\pm}^s + p_{\pm} g^{is}) \right) = \frac{1}{\mathcal{K}_m} \tilde{n} (E^s + e^{sik} v_i B_k) + \frac{2}{\mathcal{K}_f} n_+ n_- (u_-^s - u_+^s). \quad (8)$$

In these equations  $E$  and  $B$  are the electric and magnetic field,  $n_{\pm}$ ,  $p_{\pm}$ ,  $w_{\pm}$ ,  $\gamma_{\pm}$  and  $u_{\pm} = \gamma_{\pm} v_{\pm}$  are the density, pressure, relativistic enthalpy, Lorentz factor and 4-velocity of electron and positron fluids respectively,  $g^{ik}$  is the spatial metric tensor of Minkowski space time and,  $e^{ijk}$  is the Levi-Civita tensor, indexes  $s$ ,  $i$  and  $k$  correspond to three spatial direction.

In the Ohm's law,  $\tilde{n} = n_+ \gamma_+ + n_- \gamma_-$  is the total number density of charged particles as measured in the laboratory frame and  $v^i = (n_+ \gamma_+ v_+^i + n_- \gamma_- v_-^i) / \tilde{n}$  is their average velocity in this frame. The last term of the Ohm's law describes the internal friction between the fluids, which is related to resistivity.

The three dimensionless parameters in these equations are

$$\mathcal{K}_q = \frac{B_0}{4\pi e L_0 n_0}, \quad \mathcal{K}_m = \frac{m_e c^2}{e B_0 L_0}, \quad \mathcal{K}_f = \frac{m_e c}{\varkappa_f n_0 L_0}, \quad (9)$$

where  $L_0$  is the characteristic length scale, the speed of light,  $c$ , is the characteristic speed,  $B_0$  the characteristic value of magnetic (and electric) field,  $n_0$  the characteristic number density of particles and  $e$  is the electron charge. The corresponding scales for the time is  $T_0 = L_0/c$ , for the mass density  $m_e n_0$  and for the pressure and enthalpy  $m_e c^2 n_0$ ,  $\varkappa_f$  is the dynamic coefficient of friction between these fluids.

The dimensionless polytropic EOS is

$$w_{\pm} = n_{\pm} + \Gamma p_{\pm} / (\Gamma - 1). \quad (10)$$

where  $\Gamma$  is the ratio of specific heats.

In this paper we solve these equations numerically, using the code JANUS (Barkov et al. 2014). The code is based on a conservative finite-difference scheme which utilises a third order WENO interpolation (Liu et al. 1994; Yamaleev & Carpenter 2009) and a third order TVD time integration of the Runge-Kutta type (Shu & Osher 1988), thus ensuring overall third order accuracy on smooth solutions. Hyperbolic fluxes are computed using the Lax-Friedrich prescription. The magnetic field is kept near divergence-free by means of the method of generalised Lagrange multiplier (Munz et al. 2000; Dedner et al. 2002; Komissarov 2007).

### 3 HARRIS CURRENT SHEET

In the paper we study stability of the Harris current sheet using Cartesian coordinates aligned with the sheet. In these coordinates, the initial magnetic field  $\mathbf{B} = (B_x(y), 0, B_z)$ , where  $B_z$  is a uniform guide field and

$$B_x = B_{\infty} \tanh\left(\frac{y}{\delta}\right), \quad (11)$$

where  $\delta$  is the half-thickness of the current sheet and  $B_{\infty}$  is the magnetic field strength far away from the sheet. The force equilibrium of the current sheet implies the total gas pressure distribution

$$p_t = p_{\infty} + \frac{B_{\infty}^2}{8\pi} \left(1 - \tanh^2\left(\frac{y}{\delta}\right)\right). \quad (12)$$

The gas pressure in the centre of the current sheet  $p_0 = p_{\infty} + B_{\infty}^2/8\pi$ . Introducing the pressure ratio  $f_p = p_0/p_{\infty}$ , we find that

$$f_p = 1 + \beta_m^{-1}, \quad (13)$$

where  $\beta_m = 8\pi p_{\infty}/B_{\infty}^2$  is the traditional (non-relativistic) magnetisation parameter of plasma. Following previous studies, we assume that the plasma temperature is uniform and hence the particle density distribution follows that of the gas pressure.

**Table 1.** TI models. The case without guide field. Here  $\lambda$  and  $\omega_i$  are initial perturbation wavelength and perturbation grow rate respectively.

Name	Resolution	domain X	domain Y	$\lambda$	$\omega_i$
TW06	128x128	[-3,3]	[-5,5]	6	0.0
TW07	128x128	[-3.5,3.5]	[-5,5]	7	0.0
TW08	128x128	[-4,4]	[-5,5]	8	0.011
TW09	128x128	[-4.5,4.5]	[-5,5]	9	0.041
TW10	128x128	[-5,5]	[-5,5]	10	0.0603
TW11	128x128	[-5.5,5.5]	[-5,5]	11	0.077
TW12	160x128	[-6,6]	[-5,5]	12	0.085
TW14	160x160	[-7,7]	[-7,7]	14	0.095
TW20	256x256	[-10,10]	[-10,10]	20	0.100
TW30	384x256	[-15,15]	[-10,10]	30	0.089
TW40	512x256	[-20,20]	[-10,10]	40	0.079
TW80	1024x512	[-40,40]	[-20,20]	80	0.047
TW160	2048x1024	[-80,80]	[-40,40]	160	0.030
TW10h	192x192	[-5,5]	[-5,5]	10	0.0657
TW10H	256x256	[-5,5]	[-5,5]	10	0.0669

The half-thickness  $\delta$  determines the drift speed of fluids in the current sheet. From the Faraday equation we find four velocity as

$$u_-^z = \frac{cB_\infty}{8\pi\delta en_-} \operatorname{sech}^2\left(\frac{y}{\delta}\right), \quad (14)$$

where we used the charge neutrality condition  $n_- = n_+$ , and hence  $u_+ = -u_-$ .

Using  $B_\infty$ ,  $\delta$  and  $n_\infty^\pm$  as the characteristic scales  $B_0$ ,  $L_0$  and  $n_0$  of the problem, we find

$$\mathcal{K}_q = 2u_0 f_p \quad \text{and} \quad \mathcal{K}_m = \frac{1}{4\theta(f_p - 1)}, \quad (15)$$

where  $u_0$  is the magnitude of  $u_-^z$  at the centre of the current sheet and  $\theta = k_b T / m_e c^2$  is the dimensionless temperature, here  $k_b$  is Boltzmann constant. Following Cerutti et al. (2014), we use  $f_p = 10$  and  $u_0 = 0.75$  but set  $\theta = 10$  instead of  $10^8$ . The latter should not have a strong effect as in both cases the thermal energy dominates in the plasma inertia and this is indeed what has been found in the previous theoretical and numerical studies (Zelenyi & Krasnoselskikh 1979; Zenitani & Hoshino 2007). Given these values, we have  $\mathcal{K}_q = 15$  and  $\mathcal{K}_m = 0.042$ . The corresponding relativistic magnetisation parameter

$$\sigma_\infty = \frac{B_\infty^2}{4\pi w_\infty} \approx 4.4,$$

where  $w_\infty = w_{-, \infty} + w_{+, \infty}$ . Using the definitions of the plasma Larmor radius,  $\rho_0 = \theta m_e c^2 / e B_\infty$ , and the skin depth,  $d_e^2 = \theta m_e c^2 / (4\pi n_\infty e^2)$ , as in (Cerutti et al. 2014), we find  $\delta = 2.4\rho_0$  and  $\delta = 1.26d_e$ , which is similar to what they have in the setup of their PIC simulations ( $\delta = 2.7\rho_0$  and  $\delta = 1.61d_e$ )<sup>1</sup>.

## 4 SIMULATIONS

All simulations presented in this paper are two-dimensional (2D). We split them in four groups. In Sections 4.1 and 4.2, we present our studies of the tearing and drift-kink instabilities of the Harris current sheet described in Sec.3, without the guide field. The main goal is to obtain dispersion curves and compare them against the results of PIC simulations. In Sec.4.3 we investigate the role of the guide field, by studying the response of modes with highest growth rates. In all models, the ratio of specific heats,  $\Gamma = 4/3$  and Courant number  $C = 0.5$ . All physical parameters are dimensionalised using the characteristic scales  $c$ ,  $L_0 = \delta$ ,  $B_0 = B_\infty$  and  $n_0 = n_\infty$ .

In order to focus on the role of inertial terms in Ohm's law, we effectively remove the resistive term by setting  $\mathcal{K}_f = 10^{15}$ .

<sup>1</sup> The difference is probably because they used  $v_0 = \sqrt{0.6}$  and not  $v_0 = 0.6$  as stated in their paper. We realised this issue a bit too late.

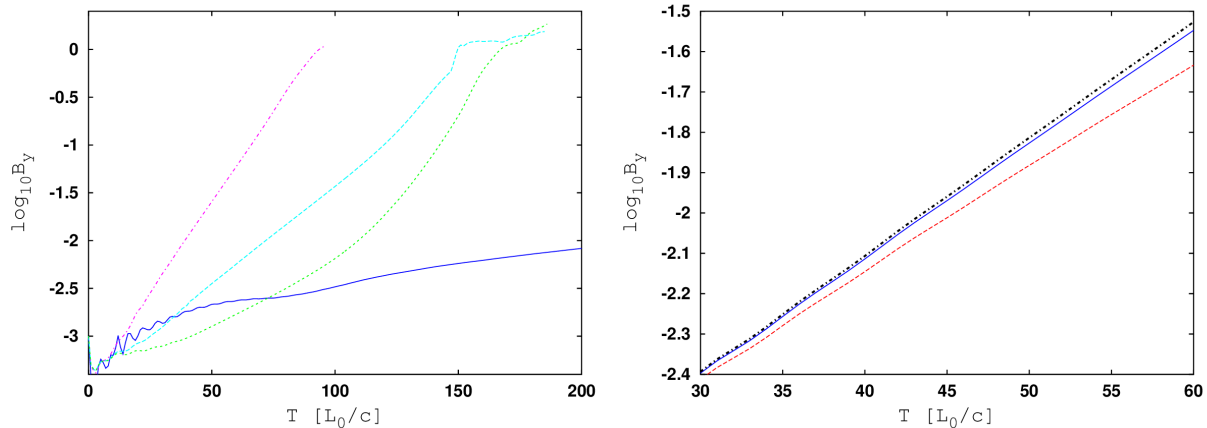


**Figure 1.** *Left panel:* Evolution of the perturbation amplitude for the models TW08 (blue solid line), TW30 (magenta dot-dashed line), TW80 (cyan dashed line) and TW160 (green dotted line). *Right panel:* Evolution of the perturbation amplitude for the models TW10 (solid line), TW10h (dashed line) and TW10H (dot-dashed line) which differ only by resolution.

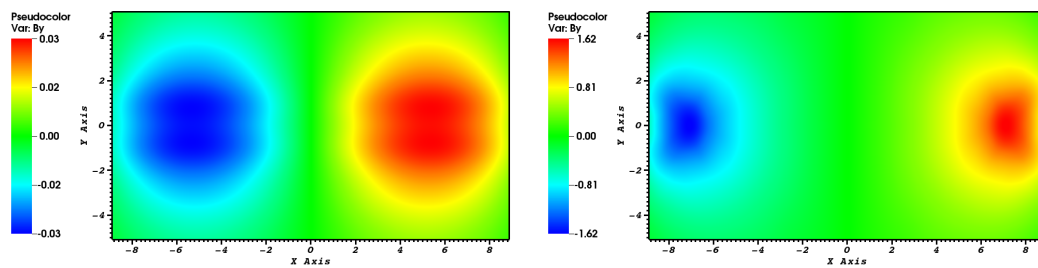


**Figure 2.** The distribution of  $B_y$  for the model TW20 at the times  $t = 23$  (top panel) and  $t = 88$  (bottom panel).

#### 4.1 Tearing instability without guide field

For the study of the tearing instability, we consider a two-dimensional problem with  $\partial_z = 0$ . The current sheet is pushed out of equilibrium by perturbing the magnetic field,  $\mathbf{B} \rightarrow \mathbf{B} + \mathbf{b}$ , where the divergence-free perturbation

$$\mathbf{b} = b_0 e^{-(y/l)^2} \left[ -\frac{2y}{(kl^2)} \cos(kx) \mathbf{i}_x + \sin(kx) \mathbf{i}_y \right], \quad (16)$$

where  $k = 2\pi/\lambda$  is the wavenumber and  $b_0 = 10^{-3}$  is the amplitude of the perturbation. In the  $x$  direction, the size of the computational domain is set to be exactly one wavelength of the perturbation and we employ the periodic boundary conditions at the  $x$  boundaries. In the  $y$ -direction, we have a comparable size of the computational domain and use the free-flow boundary conditions. The basic parameters of the simulations are given in the Table 1.

To quantify the perturbation amplitude we use the maximum value of  $B^y$  in the computational domain. Figure 1 shows examples of the amplitude evolution for a number of models. As the initial perturbation is not a normal mode of the instability, it leads to excitement not only of the normal mode with the wavelength equal to the  $x$  size of the computational box, the fundamental mode, but also its overtones as well as and propagating waves. The latter are partially transmitted through the  $y$  boundaries of the computational box and do not grow in amplitude. Soon they become dominated by the unstable normal modes. When the wavelength of the fundamental mode is below the maximum of the dispersion curve, it completely dominates the evolution as the parasitic overtones grow slower. This is illustrated in Figure 2.

When the wavelength of the fundamental mode is above the maximum, the evolution is more complicated. Initially, it dominates overtones simply because its initial amplitudes is higher. However, some parasitic overtones may now grow faster and eventually overtake it while still at the linear phase. In the amplitude plots, this is manifested by an increase of the curve gradient, as exhibited by the curve of the TW160 model in Figure 1. In the 2D plots of the solution, this is manifest by the appearance of dominant small scale structures (see Figure 3). This has to be taken into account when measuring the growth rate of the fundamental mode.

We have checked the convergence of our numerical results by comparing the data obtained with different numerical resolutions. The right panel of Figure 1 shows the results for the model TW10 obtained with  $128 \times 128$  cells,  $192 \times 192$  cells (TW10h) and  $256 \times 256$  (TW10H), which clearly indicate their convergence. Base on the study we conclude the numerical error of our growth rates does not exceed 10%.

The growth rates,  $\omega_i$ , of the fundamental modes are collected in Table 1 and Figure 4. The results agree with the

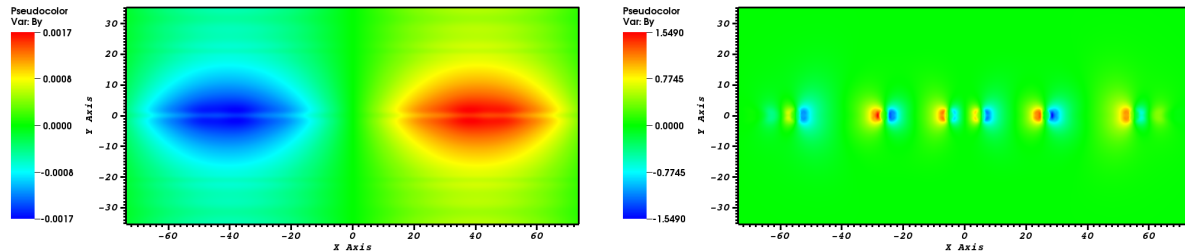


**Figure 3.** The distribution of  $B_y$  for the model TW160 at the times  $t = 60$  (top panel) and  $t = 180$  (bottom panel). One can see that initially it is the original perturbation of the wavelength equal to the domain length in the  $x$  direction which dominates. However, at later times shorter wavelengths begin to dominate.

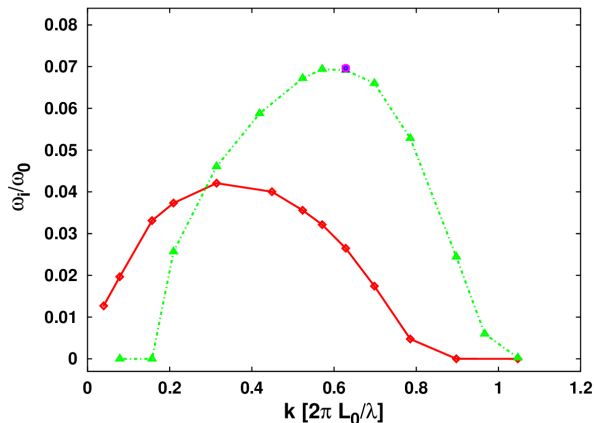


**Figure 4.** Growth rates of TI (thick red solid line) and DKI (green thick dot-dashed line) modes in the current sheet without guide field. The magenta circle shows the result obtained with doubled numerical resolution.

theoretical models which predict instability for  $0 < k < 1$  with a peak at  $k \approx 0.5$  (Zelenyi & Krasnoselskikh 1979; Pétri & Kirk 2007). The PIC simulations show a broader dispersion curve, with unstable modes existing beyond  $k = 1$  and the peak growth rate  $\omega_i/\omega_0 \approx 0.045$ , where  $\omega_0 = \theta m_e c/eB$ , at  $k \approx 0.58$  (Cerutti et al. 2014). In our simulations, the peak is more pronounced and located at  $k \approx 0.3$ . In order to compare our results, we note that with our scaling  $\omega_0^{-1} = \theta \mathcal{K}_m = 0.42$  and thus  $\omega_i/\omega_0 \approx 0.04$ . Overall, we conclude that our results agree quite well with the PIC data.

#### 4.2 Drift-kink instability without guide field

For the study of the drift-kink instability, we consider a two-dimensional problem with  $\partial_x = 0$ . The current sheet is pushed out of equilibrium by perturbing the velocity field of both the electron and positron fluids,  $\mathbf{U} \rightarrow \mathbf{U} + \mathbf{u}$ , where

$$\mathbf{u} = u_0 \cos(kz) \hat{\mathbf{i}}_y, \quad (17)$$

with  $u_0 = 10^{-3}$ . Like in the tearing simulations, the size of the computational domain in the  $z$  direction is set to be exactly one wavelength of the perturbation and we employ relevant periodic boundary conditions at the  $z$  boundaries. In the  $y$ -direction, we have a comparable size and use the free-flow boundary conditions. The basic parameters of the simulations are given in the Table 2.

The left panel of Figure 5 illustrates the structure of the unstable modes across the current sheet in our simulations. These results are in a good agreement with the structure of normal modes found in the linear theory of DK instability Zenitani & Hoshino (2007). We quantify the perturbation amplitude using the maximum value of  $|u_+^y|$  in the computational box. The right panel of Figure 5 shows typical examples of its evolution in the simulations.

Figure 4 shows the dispersion curve. Like in the tearing instability, the dispersion curve of DKI has a clear maximum and in the simulations with longer wavelengths, faster growing parasitic overtone modes can outperform the fundamental mode. In such cases, we compute  $\omega_i$  only for the initial part of the amplitude curve, where the fundamental mode is still dominant. In order to verify that the numerical resolution is sufficient and the growth rates are trustworthy, we have carried out a separate convergence study. For example, we repeated the simulations KW10 with higher resolution:  $192^2$  (model KW10h) and  $256^2$  (model KW10H). The results indicate that the growth rate error for the model KW10 is below 1% (see Table 2).

**Table 2.** DKI models. The case without guide field.

Name	Resolution	Domain Z	Domain Y	$\lambda$	$\omega_i$
KW06	128x128	[-3,3]	[-5,5]	6	0.0
KW065	128x128	[-3.25,3.25]	[-5,5]	6.5	0.0
KW07	128x128	[-3.5,3.5]	[-5,5]	7	0.058
KW08	128x128	[-4,4]	[-5,5]	8	0.135
KW09	128x128	[-4.5,4.5]	[-5,5]	9	0.159
KW10	128x128	[-5,5]	[-5,5]	10	0.165
KW11	128x128	[-5.5,5.5]	[-5,5]	11	0.1646
KW12	192x128	[-6,6]	[-5,5]	12	0.160
KW15	192x128	[-7.5,7.5]	[-5,5]	15	0.137
KW20	256x128	[-10,10]	[-5,5]	20	0.110
KW30	384x256	[-15,15]	[-10,10]	30	0.061
KW40	512x256	[-20,20]	[-10,10]	40	0.0
KW80	1024x512	[-40,40]	[-20,20]	80	0.0
KW10h	192x192	[-5,5]	[-5,5]	10	0.16553
KW10H	256x256	[-5,5]	[-5,5]	10	0.16581

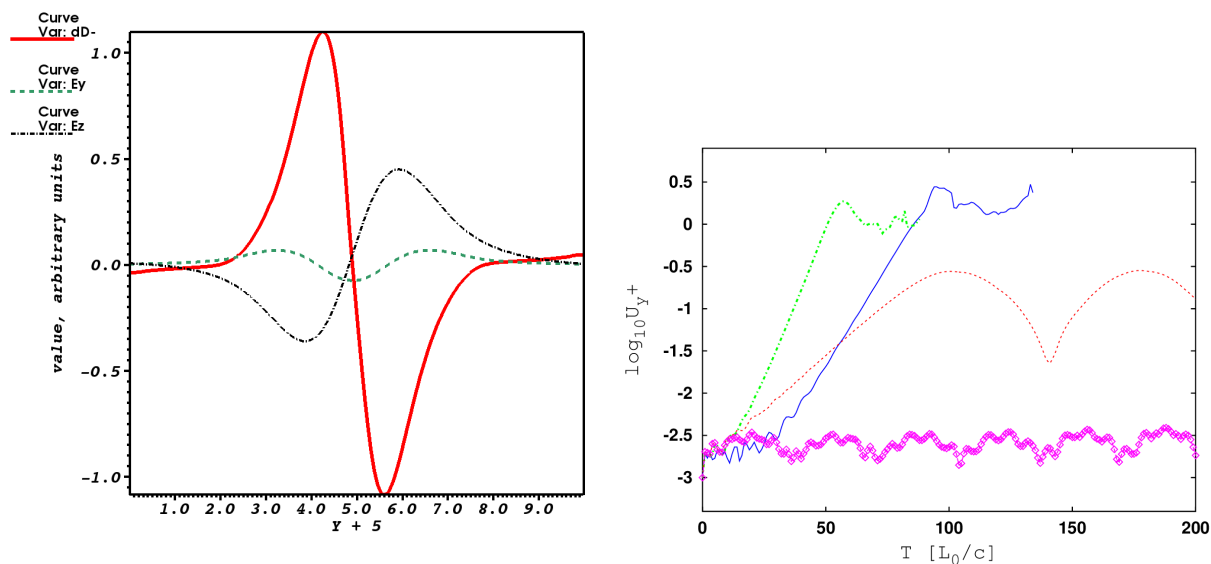


**Figure 5.** *Left panel:* Structure of DK-modes without guide field. The lines show the perturbation of electron density (solid red line),  $E_y \times 30$  (dashed green line) and  $E_z \times 30$  (dash-dotted black line) as found in the model KW09. The measurements are taken at  $t = 66$  along the line  $z = 2$ . *Right panel:* Growth of DK modes without guide field. The curves represent models KW065 (magenta dashed line with diamonds), KW07 (red dotted line), KW10 (green dot-dashed line) and KW20 (blue solid line). The shown quantity is the maximum value of  $u_+^y$  in the computational box.

Like in the tearing instability, the unstable modes occupy the range  $0 < k < 1$ , though the long wavelength modes with  $k < 0.2$  appear to be suppressed (see Figure 4). In the PIC simulations the instability occurs even for  $k > 1$  but at a lower growth rate (Zenitani & Hoshino 2007; Cerutti et al. 2014). In our simulations, the growth rate peaks at  $k_{\max} \approx 0.6$ , where it reaches the value  $\omega_{\max} \approx 0.16$ . Both Zenitani & Hoshino (2007) whereas in the PIC simulations  $k_{\max} \approx 0.7$  and  $\omega_{\max} \approx 0.13$  (Zenitani & Hoshino 2007; Cerutti et al. 2014). Thus the results of two-fluid and PIC simulations agree with each other quite well again. The linear analysis of Zenitani & Hoshino (2007) shows that the instability domain extends beyond  $k = 1$ . However this theoretical results is not trustworthy as it is obtained using the long-wavelength approximation,  $k \ll 1$ .

Interestingly, the short-wavelength modes appear to be non-decaying periodic or quasi-periodic oscillations. The model KW065 is one such example. Its amplitude remains on the level of initial perturbation. The model KW07 seems to be a transitional case, where the initial phase of exponential growth terminates at a relatively low amplitude and is followed by oscillations.

In the PIC simulations, the non-linear phase of DKI is characterised by magnetic dissipation, plasma heating, and widening of the current sheet. All these properties are observed in our simulations as well. Moreover, we find that shock waves develop in electron and positron fluids ( see Figure 6) and they play an important role in plasma heating.

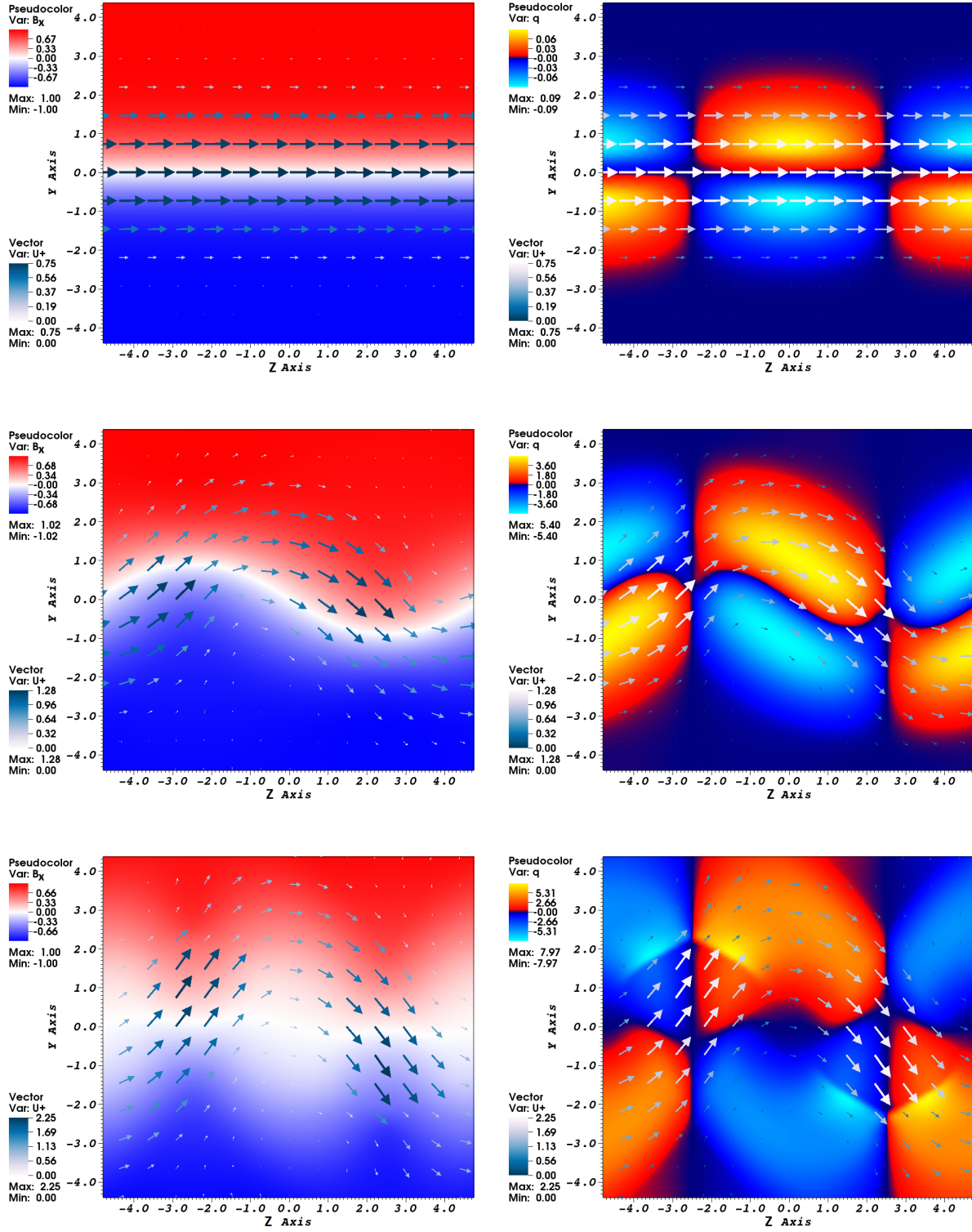


**Figure 6.** Development of the drift-kink instability in the model KW10. In the left panels, the coloured image shows the distribution of the out-of-the-plane component of magnetic field  $B_x$  and in the right panels, the distribution of electric charge. The arrows show the velocity field of positrons. The simulation time is  $t = 20, 50$  and  $58$  (from top to bottom). By the time  $t = 58$ , a significant fraction of magnetic energy has been dissipated and shock waves developed in the electron and positron fluids.



**Table 3.** The full set of models with guide field in the study of DKI.

Name	Resolution	Domain Z	Domain Y	$\lambda$	$\alpha_{\text{gf}}$	$\omega_i$
Ka09W05	192x192	[-2.5,2.5]	[-5,5]	5	0.9	0.0
Ka09W055	192x192	[-2.75,2.75]	[-5,5]	5.5	0.9	0.064
Ka09W06	192x192	[-3.0,3.0]	[-5,5]	6	0.9	0.107
Ka09W07	192x192	[-3.5,3.5]	[-5,5]	7	0.9	0.128
Ka09W08	192x192	[-4.0,4.0]	[-5,5]	8	0.9	0.113
Ka09W09	192x192	[-4.5,4.5]	[-5,5]	9	0.9	0.092
Ka09W10	192x192	[-5.0,5.0]	[-5,5]	10	0.9	0.054
Ka09W12	192x192	[-6.0,6.0]	[-5,5]	12	0.9	0.0
<hr/>						
Ka12W04	192x192	[-2.0,2.0]	[-5,5]	4	1.2	0.0
Ka12W045	192x192	[-2.25,2.25]	[-5,5]	4.5	1.2	0.0
Ka12W05	192x192	[-2.5,2.5]	[-5,5]	5	1.2	0.079
Ka12W055	192x192	[-2.75,2.75]	[-5,5]	5.5	1.2	0.106
Ka12W06	192x192	[-3.0,3.0]	[-5,5]	6	1.2	0.104
Ka12W065	192x192	[-3.25,3.25]	[-5,5]	6.5	1.2	0.086
Ka12W07	192x192	[-3.5,3.5]	[-5,5]	7	1.2	0.0
<hr/>						
Ka16W038	192x192	[-1.9,1.9]	[-5,5]	3.8	1.6	0.0
Ka16W04	192x192	[-2.0,2.0]	[-5,5]	4	1.6	0.037
Ka16W045	192x192	[-2.25,2.25]	[-5,5]	4.5	1.6	0.068
Ka16W05	192x192	[-2.5,2.5]	[-5,5]	5	1.6	0.050
Ka16W055	192x192	[-2.75,2.75]	[-5,5]	5.5	1.6	0.017
Ka16W06	192x192	[-3.0,3.0]	[-5,5]	6	1.6	0.0

### 4.3 Current sheets with guide field

Following Zenitani & Hoshino (2008) and Cerutti et al. (2014) we first study the effect of guide field on the fastest growing modes in the case without the the guide field. In our study, these are  $k \approx 0.31$  ( $\lambda = 20$ ) for TI and  $k \approx 0.63$  ( $\lambda = 10$ ) for DKI. The computational domain is  $[-5, 5] \times [-5, 5]$  with  $128 \times 128$  cells for the TI simulations and  $[-10, 10] \times [-5, 5]$  with  $256 \times 128$  cells for the DKI simulations. The strength of the guide field is described by the parameter  $\alpha_{\text{gf}} = B_z/B_\infty$ . The perturbations are introduced in exactly the same way as in the models without the guide field.

The results are shown in Figure 7. As in the previous studies, the guide field makes a stronger impact on the DKI mode than on the TI mode. For the TI mode, we find that the growth rate is reduced by 50% only at  $\alpha_{\text{gf}} = 5$ , which is in agreement with the two-fluid linear analysis by Zenitani & Hoshino (2008) and their PIC simulations. The PIC simulations by Cerutti et al. (2014) show a somewhat stronger effect, with a 45% reduction already at  $\alpha_{\text{gf}} = 1$ . However, their curve is not monotonic, which may indicate higher numerical errors. As to the DKI mode, we find that it is totally suppressed when  $\alpha_{\text{gf}} > 1$ . This is in a good agreement with the linear stability analysis of Zenitani & Hoshino (2008), who find that for the DKI mode with  $k = 0.7$  the critical guide field is  $\alpha_{\text{gf},c} \approx 0.5$ , which also agrees with the results of their PIC simulations. Based on their PIC simulations, Cerutti et al. (2014) find  $\alpha_{\text{gf},c} \approx 0.8$  for  $k = 0.67$ , which is even closer to our results.

Given the strong effect of the guide field on the drift-kink instability, we have carried out additional simulations with the aim to clarify the dependence of the DKI dispersion curve on the guide field strength. The parameters of these simulations are given in Table 3 and their results are illustrated in Figure 7. The surprising result is that the growth rate is not uniformly reduced for all wavelengths. As the guide field increases, the peak of the curve does get lower but in addition the unstable range shifts towards shorter wave lengths. As a result, some modes which grow at  $\alpha_{\text{gf}} = 0$  become completely stabilised for  $\alpha_{\text{gf}} \neq 0$  and the other way around (see the right panel of Figure 7). The blue line in the left panel of Figure 7 shows the dependence of the maximal growth rate on  $\alpha_{\text{gf}}$ .

## 5 CONCLUSION

In this work we studied the tearing and drift-kink instabilities of current sheets in collisionless electron-positron plasma by means of 2D two-fluid computer simulations. We set the internal friction (resistivity) to zero and considered current sheets of thickness comparable to the electron skin depth, so that the inertial terms of the generalised Ohm's law become significant. Our results are compared with those of the PIC simulations carried out by other researches for current sheets with similar parameters. We find that there is a good overall agreement between the two-fluid and PIC simulations. In both cases, the fastest growing modes have very similar wavelengths and growth rates when the guide field is small. In both cases, the guide field reduces the growth rates of unstable modes. There are some differences too. For example, the unstable range of both TI and DKI appears to be somewhat narrower and the guide field has a weaker stabilising effect on the TI mode in the two-fluid simulations. We also find that, in addition to getting lower, the dispersion curve of DKI also shifts towards higher

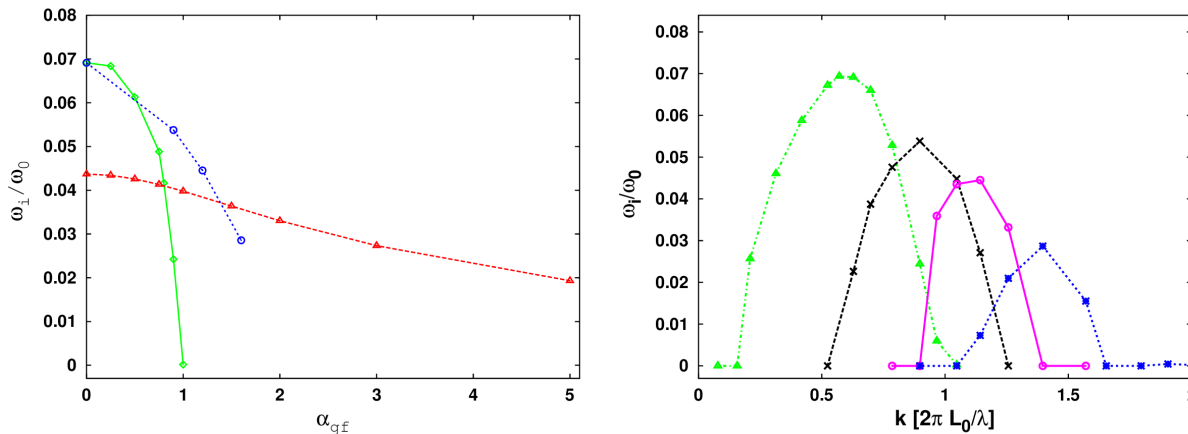


**Figure 7.** *Left panel:* Dependence of the growth rates of the tearing and drift-kink instabilities on the strength of guide field,  $\alpha_{gf} = B_z/B_\infty$ . The red line shows the TI mode with  $k \approx 0.3$  ( $\lambda = 20$ ) and the green line the DKI mode with  $k \approx 0.6$  ( $\lambda = 10$ ). The blue line shows the growth rate for the fastest growing DKI mode (its wavelength depends on  $\alpha_{gf}$ ). *Right panel:* Growth rates of the drift-kink instability in the presence of the guide field. The lines are the dispersion curves for  $\alpha_{gf} = 0$  (green triangles), 0.9 (black crosses), 1.2 (magenta squares) and 1.6 (magenta stars).

wavenumbers when the guide fields gets stronger. We cannot say if this is in agreement with the PIC simulations due to the lack of relevant PIC data.

It would be naive to hope that the two-fluid simulations could exactly reproduce the results of PIC simulations, and they do not. However, the differences appear to be rather minor. This suggests that the two-fluid model can adequately describe the macroscopic dynamics of plasma with collisionless currents sheets, yielding sufficiently accurate magnetic reconnection rates. In order to confirm this we have started a study of 2D magnetic reconnection in the plasmoid dominated regime. The preliminary results are encouraging.

## 6 ACKNOWLEDGMENTS

The simulations have been carried out either on a work station with multi-core processors or/and on the CFCA cluster (XC30) of National Astronomical Observatory of Japan. We make 2D visualisation and analysis using package VisIt (Childs et al. 2012) and Octave. SSK acknowledges support by STFC under the standard grant EP/N023986/1. BMV acknowledge partial support by JSPS (Japan Society for the Promotion of Science): No.2503786, 25610056, 26287056, 26800159. BMV also MEXT (Ministry of Education, Culture, Sports, Science and Technology): No.26105521 and RFBR grant 12-02-01336-a.

## REFERENCES

- Amano T., Kirk J. G., 2013, *ApJ*, 770, 18  
 Barkov M., Komissarov S. S., Korolev V., Zankovich A., 2014, *MNRAS*, 438, 704  
 Bessho N., Bhattacharjee A., 2012, *ApJ*, 750, 129  
 Bhattacharjee A., Huang Y.-M., Yang H., Rogers B., 2009, *Physics of Plasmas*, 16, 112102  
 Biskamp D., 1986, *Physics of Fluids*, 29, 1520  
 Cerutti B., Werner G. R., Uzdensky D. A., Begelman M. C., 2014, *ApJ*, 782, 104  
 Childs H., Brugger E., Whitlock B., Meredith J., Ahern S., Pugmire D., Biagas K., Miller M., Harrison C., Weber G. H., Krishnan H., Fogal T., Sanderson A., Garth C., Bethel E. W., Camp D., Rubel O., Durant M., Favre J. M., Navratil P., 2012, in , *High Performance Visualization—Enabling Extreme-Scale Scientific Insight*. pp 357–372  
 Dedner A., Kemm F., Kroner D., Munz C.-D., Schnitzer T., Wesenberg M., 2002, *J. Chem. Phys.*, 115, 200  
 Drenkhahn G., Spruit H. C., 2002, *A&A*, 391, 1141  
 Gurovich V. T., Solov’ev L. S., 1986, *JETP*, 91, 1144  
 Kojima Y., Oogi J., 2009, *MNRAS*, 398, 271  
 Komissarov S. S., 2007, *MNRAS*, 382, 995  
 Komissarov S. S., 2013, *MNRAS*, 428, 2459  
 Liu X.-D., Osher S., Chan T., 1994, *J. Chem. Phys.*, 115, 200  
 Liu Y.-H., Guo F., Daughton W., Li H., Hesse M., 2015, *Physical Review Letters*, 114, 095002  
 Loureiro N. F., Schekochihin A. A., Cowley S. C., 2007, *Physics of Plasmas*, 14, 100703  
 Lyutikov M., Blandford R., 2003, *arXiv:astro-ph/0312347*  
 McKinney J. C., Uzdensky D. A., 2012, *MNRAS*, 419, 573

- Munz C.-D., Omnes P., Schneider R., Sonnendrücker E., Voß U., 2000, *J. Chem. Phys.*, 161, 484  
Pétri J., Kirk J. G., 2007, *Plasma Physics and Controlled Fusion*, 49, 1885  
Porth O., Komissarov S. S., Keppens R., 2013, *MNRAS*, 431, L48  
Porth O., Komissarov S. S., Keppens R., 2014, *MNRAS*, 438, 278  
Romanova M. M., Lovelace R. V. E., 1992, *A&A*, 262, 26  
Shibata K., Tanuma S., 2001, *Earth, Planets, and Space*, 53, 473  
Shu C.-W., Osher S., 1988, *J. Chem. Phys.*, 77, 439  
Sironi L., Spitkovsky A., 2014, *ApJ*, 783, L21  
Uzdensky D. A., Loureiro N. F., Schekochihin A. A., 2010, *Physical Review Letters*, 105, 235002  
Yamaleev N. K., Carpenter M. H., 2009, *J. Chem. Phys.*, 228, 3025  
Zelenyi L. M., Krasnoselskikh V. V., 1979, *Soviet Ast.*, 23, 460  
Zenitani S., Hesse M., Klimas A., 2009a, *ApJ*, 705, 907  
Zenitani S., Hesse M., Klimas A., 2009b, *ApJ*, 696, 1385  
Zenitani S., Hoshino M., 2001, *ApJ*, 562, L63  
Zenitani S., Hoshino M., 2007, *ApJ*, 670, 702  
Zenitani S., Hoshino M., 2008, *ApJ*, 677, 530  
Zhang B., Yan H., 2011, *ApJ*, 726, 90